

# Modeling the complete prevention of disruption-generated runaway electron beam formation with a passive 3D coil in SPARC

RA Tinguely<sup>1</sup>, VA Izzo<sup>2</sup>, DT Garnier<sup>1</sup>, A Sundström<sup>3</sup>, K Särkimäki<sup>4</sup>,

O Embréus<sup>3</sup>, T Fülöp<sup>3</sup>, RS Granetz<sup>1</sup>, M Hoppe<sup>3</sup>, I Pusztai<sup>3</sup>, and R Sweeney<sup>1</sup>

<sup>1</sup>*Plasma Science and Fusion Center, Massachusetts Institute of Technology, Cambridge, MA 01239, USA*

<sup>2</sup>*Fiat Lux, San Diego, CA 92101, USA*

<sup>3</sup>*Department of Physics, Chalmers University of Technology, SE-41296 Göteborg, Sweden and*

<sup>4</sup>*Max Planck Institute for Plasmaphysics, 85748 Garching, Germany*

The potential formation of multi-mega-ampere beams of relativistic “runaway” electrons (REs) during sudden terminations of tokamak plasmas poses a significant challenge to the tokamak’s development as a fusion energy source. Here, we use state-of-the-art modeling of disruption magnetohydrodynamics coupled with a self-consistent evolution of RE generation and transport to show that a non-axisymmetric in-vessel coil will *passively* prevent RE beam formation during disruptions in the SPARC tokamak, a compact, high-field, high-current device capable of achieving a fusion gain  $Q > 2$  in deuterium-tritium plasmas.

Keywords: Runaway electron, plasma disruption, tokamak, mitigation

*Introduction.*—The tokamak, a magnetic confinement fusion device, is perhaps the most promising concept extrapolating to a future fusion power plant. Yet it is not without an Achilles’ heel: A disruption is the sudden, often unplanned termination of a plasma discharge caused by a host of instabilities [1, 2]. While instability limits can be avoided so that disruptions occur with low probability, tokamaks must be designed to mitigate disruptions’ deleterious effects.

This paper focuses on the mitigation of so-called “runaway” electrons (REs). The sudden cooling of a plasma during the disruption’s thermal quench (TQ) leads to an increase in the plasma resistivity  $\propto T^{-3/2}$ , with  $T$  the plasma temperature. In an attempt to maintain the pre-disruption plasma current, a large electric field is induced, accelerating electrons continuously against a decreasing collisional friction  $\propto v^{-2}$ , with  $v$  the electron speed. The RE population is exponentially amplified by the same avalanche process proposed for atmospheric breakdown during lightning [3], and the resulting RE beam, carrying currents of order MA and with individual electron energies of order MeV, can be destructive if not avoided or mitigated [4, 5].

The most studied mitigation method is massive material injection (gas or shattered pellet) either before or after RE beam formation [6–9]. RE avoidance has also been pursued via applied 3D magnetic fields, with the resulting stochasticity transporting REs out of the plasma [10–17]. While initial results are promising, fully stochastic fields have not yet been achieved [18, 19], and this is still an *active* mitigation scheme.

In this work, we demonstrate complete prevention of disruption-generated REs in the SPARC tokamak [20] via a *passive* mitigation strategy. A conducting coil with 3D structure – the RE Mitigation Coil (REMC) – is energized by the disruption-induced voltage, and the resulting magnetic field stochasticity causes electrons to be lost faster than a RE beam can form [19, 21]. In this Letter, we focus on the worst-case scenario, a dis-

ruption of the “primary reference discharge” (PRD): a deuterium-tritium, H-mode plasma with major/minor radii  $R_0 = 1.85\text{ m}/a = 0.57\text{ m}$ , toroidal magnetic field  $B_0 = 12.2\text{ T}$ , plasma current  $I_p = 8.7\text{ MA}$ , volume-averaged density  $\langle n \rangle \approx 3 \times 10^{20}\text{ m}^{-3}$  and temperature  $\langle T \rangle \approx 7\text{ keV}$ , and fusion power  $P_{\text{fus}} = 140\text{ MW}$ . We assess the efficiency of REMC by first computing its vacuum magnetic field perturbation, which is then included in 3D magnetohydrodynamics (MHD) modeling; in the resulting fields, RE orbits are traced to calculate transport coefficients for a fluid-kinetic solver of RE generation and transport.

*Vacuum field modeling.*—All toroidally continuous, conducting structures in the SPARC tokamak are modeled with the 3D finite element code COMSOL [22]: the central solenoid, double-walled vacuum vessel (VV), passive stability plates, and poloidal field, divertor, and vertical stability (VS) coils [2, 20]. The copper-based  $n = 1$  REMC is situated at the outboard VV wall with two vertical legs avoiding ports and two horizontal legs near the VS coils (see Fig. 12(a) of [2]). An elliptical toroid of uniform current density approximates the post-TQ redistribution of plasma current, and a linear decay over 3.2 ms simulates the fastest expected current quench (CQ) from empirical scalings [2, 23]. The mutual inductance between the plasma and REMC leads to a nearly linear ramp in REMC current; the peak value  $I_{\text{coil}} = 590\text{ kA}$  is the maximum achievable current (driven passive-inductively) using this particular coil placement and resistivity. The result is  $I_p$ -dependent vacuum magnetic perturbations, along with the magnetic energy available for dissipation during the CQ.

Figure 1 shows the poloidal ( $m$ ) spectrum in straight field-line coordinates of the dominant  $n = 1$  vacuum magnetic field - specifically the component normal to the PRD’s flux surfaces - at maximum  $I_{\text{coil}}$ . As expected, the spectrum is symmetric around  $m = 0$ , and the position of peak amplitude moves inward (farther from the REMC) with decreasing  $|m|$ . While the vacuum field does not

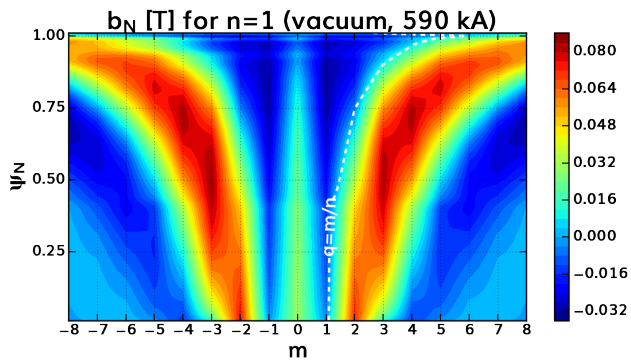


FIG. 1. Poloidal spectrum of  $n = 1$  vacuum magnetic perturbations from the REMC at maximum current: the amplitude  $b_N$  (T) normal to (normalized) flux surface  $\psi_N$  vs poloidal mode number  $m$ , with safety factor profile  $q$  overlaid (dashed).

appear to be resonant with this particular safety factor profile  $q$ , field distributions like this are expected to drive the strongest kink response of the plasma and thereby the strongest resonant fields [24]. This is evident in the results of MHD modeling in the next section.

*3D MHD modeling.*—The NIMROD 3D MHD code [25] is used to model only the CQ phase of the disruption, with external 3D magnetic fields from COMSOL. Only the surface normal components of the  $n = 1-10$  toroidal Fourier modes are applied at the location of the NIMROD simulation boundary. NIMROD has previously been run with applied time-changing boundary fields to model the application of resonant magnetic perturbations in the DIII-D tokamak [26]. The present model differs only in that the amplitudes’ time-dependence is not specified *a priori*; rather, it is calculated in proportion to the  $I_p$  decay as the simulation evolves, using the value of the maximum REMC current (590 kA) from COMSOL:

$$I_{\text{coil}}(t) = \max(I_{\text{coil}}) \times [1 - I_p(t)/I_p(t=0)].$$

Beginning with an 8.7 MA steady-state SPARC equilibrium [27], a CQ is initiated via an artificially induced TQ wherein the coefficient of perpendicular thermal conductivity is set to a large value,  $4 \times 10^4 \text{ m}^2/\text{s}$ , for only the first 0.045 ms of the simulation, until essentially all of the thermal energy is lost; then it is reduced to a more modest  $2 \text{ m}^2/\text{s}$ . A more realistic TQ induced by impurity radiation has shown significant losses of REs in SPARC [2], but the present artificial-TQ method conservatively bypasses any TQ MHD and only considers the CQ.<sup>1</sup> Once the plasma is cold and the thermal diffusivity is reduced, a balance of Ohmic heating and radiation

from  $4.8 \times 10^{21}$  atoms of added Neon determines the CQ temperature,  $T \approx 3-8 \text{ eV}$  from the plasma edge to core.

As  $I_p$  begins to decay and the external fields grow, odd mode numbers are predominantly perturbed by the REMC (Fig. 2(a,b)). Nonlinear growth of every mode is quickly excited, saturating around  $t \approx 0.65 \text{ ms}$ , with  $n = 2$  being the second largest mode after  $n = 1$ . The  $n = 1$  and 2 saturated, nonlinear modes include many poloidal harmonics of comparable amplitude, with  $m/n = 1/1, 2/1,$  and  $3/2$  modes prominent near the core (Fig. 2(c,d)). The growth of these modes is responsible for a redistribution of the current density profile, producing a small inflection in the  $I_p$  decay as the plasma internal inductance  $\ell_i$  decreases. Near-complete destruction of magnetic flux surfaces occurs shortly after ( $t \approx 0.7 \text{ ms}$ ), but a small island, with width of order cm, reappears in the core within  $t = 0.5 \text{ ms}$  and continues to slowly grow even as the amplitude of the external fields further increases (Fig. 2(e-g)). Therefore, global magnetic field stochasticity is achieved temporarily by a combination of the applied external fields and the excitement of nonlinear MHD mode growth.

*Evaluation of transport coefficients.*—The orbit-following code ASCOT5 [28] is used to compute the advection and diffusion coefficients ( $A, D$ ) characterizing the radial transport of electrons in the 3D stochastic fields from NIMROD. Markers are traced in stationary timeslices, initialized with different radial positions  $r$ , momenta  $p$  (normalized by the electron mass  $m_e$  and speed of light  $c$ ), and pitches  $p_{\parallel}/p$ . The transport is assumed to be dominated by the field stochasticity, and therefore collisions and electric field acceleration are not included<sup>2</sup>. This numerical scheme is used because the alternative, Rechester-Rosenbluth diffusion [29], does not accurately portray transport in fields perturbed by external coils [30, 31] and also omits finite-orbit-width (FOW) effects that can reduce RE transport ( $\propto p^{-1}$ ) at sufficiently high energy [32, 33].

The method of evaluating the transport coefficients is adopted from an earlier scheme [34] and described in [31]. At the beginning of the orbit-following simulation, markers are assigned ( $r/a, p, p_{\parallel}/p$ ) values and random toroidal positions. They are then traced for 0.02 ms or until they pass the separatrix, and each time a marker crosses the outer midplane its position is recorded. For markers that remain confined, the time-evolution of the recorded radial positions is used to estimate  $A$  and  $D$ . For markers that are lost, the loss-times are used to fit the “first passage time distribution,” with  $A$  and  $D$  fitted parameters. Finally, the mean value is taken from the marker-specific coefficients to represent  $A$  and  $D$  at that position in phase space.

<sup>1</sup> Though not shown here, a NIMROD simulation including the artificial TQ and *not* including the REMC results in *no* CQ MHD, meaning that the MHD observed here is solely due to the coil.

<sup>2</sup> The impact of magnetic islands on transport are not considered in ASCOT5 calculations, but are incorporated in some DREAM simulations.

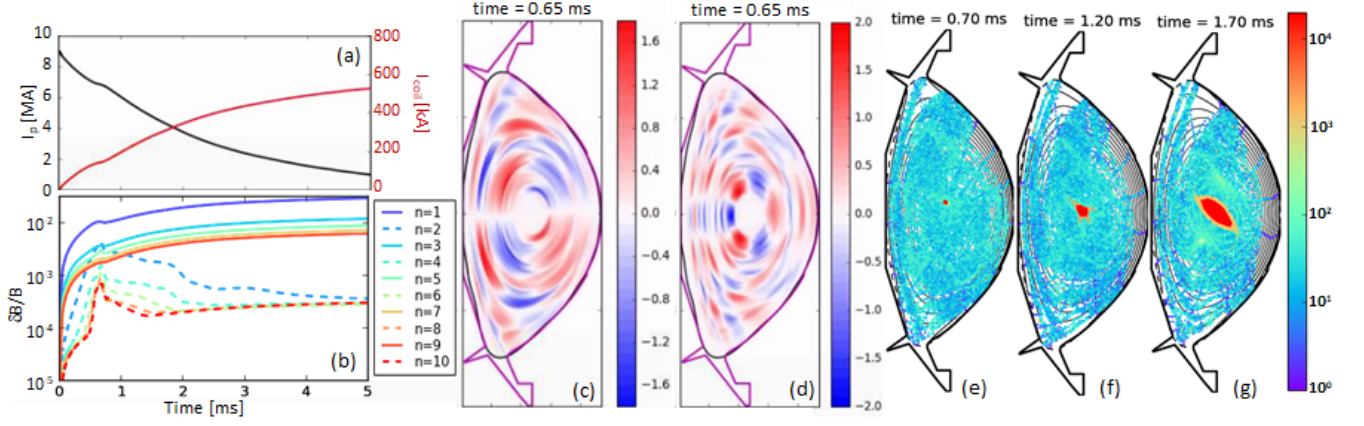


FIG. 2. NIMROD simulation results for the  $n = 1$  REMC: (a) plasma current and coil current vs time; (b) amplitude of  $n = 1-10$  modes in units of  $\delta B/B = \sqrt{W_{\text{mag}}(n)/W_{\text{mag}}(n=0)}$ ; (c)  $n = 1$  and (d)  $n = 2$  toroidal current densities ( $\text{MA}/\text{m}^2$ ) at the time of nonlinear mode saturation (with black line the simulation boundary and magenta line the SPARC first wall shape); (e–g) magnetic field line Poincaré plots on top of poloidal flux contours, where colors represent the number of toroidal transits before exiting or reaching the maximum integration length of 20,000. The empty regions near the boundary in (e–g) are artifacts of short field lines that quickly exit the volume.

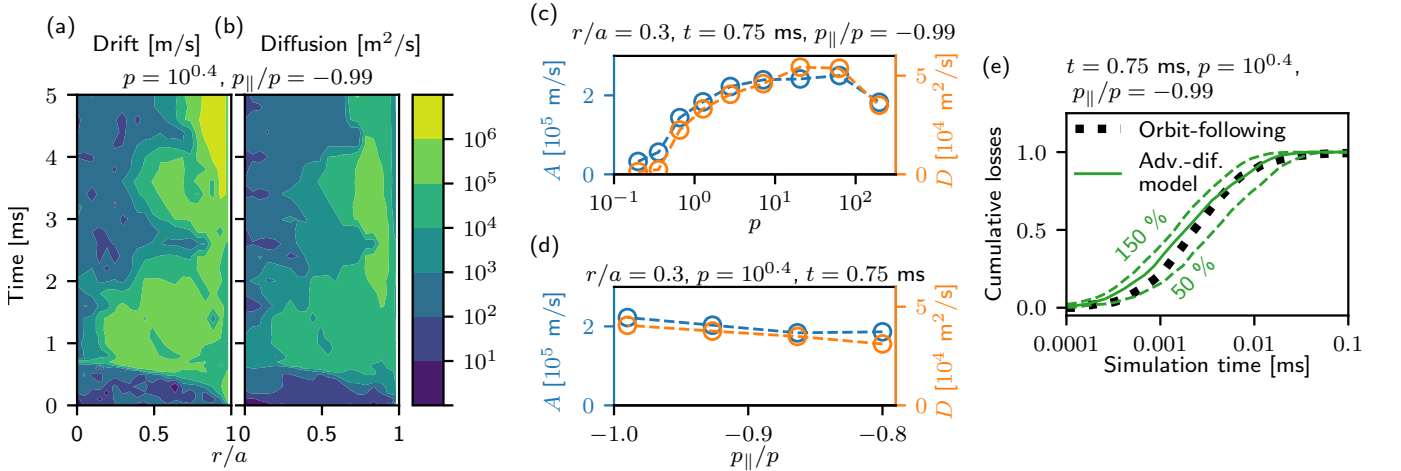


FIG. 3. (a–d): Transport coefficients as a function of (a,b) time and radius, (c) normalized momentum, and (d) pitch. The circles in (c) and (d) indicate the coordinates at which the coefficients were evaluated. (e) The cumulative fraction of markers lost as a function of simulation time computed with the advection–diffusion model (green) compared to the equivalent orbit-following ASCOT5 simulation (dotted black). Dashed green lines in (e) correspond to cases when the coefficients are scaled by factors 150% / 50% of the nominal value (solid green). Fixed values are given above each plot.

Samples of evaluated coefficients are shown in Fig. 3(a–d). The time-interval over which stochastic fields reach and persist in the core ( $t \approx 0.7-2.0$  ms) is reflected in the transport coefficients. During this time,  $A \sim 10^5$  m/s and  $D \sim 10^4$   $\text{m}^2/\text{s}$ . The transport grows initially with momentum, but decreases for  $p > 10^2$  ( $E > 50$  MeV), likely due to FOW effects. Likewise, the pitch dependency is linear except when the electron energies are high and FOW effects again become relevant. However, as described in the next section, most REs are expected to attain energies  $< 20$  MeV, thereby minimizing these effects.

Figure 3(e) shows accumulated losses when the advection-diffusion equation is solved numerically using

the evaluated coefficients. Here, the initial population consists of electrons uniformly distributed radially. To confirm the validity of modeling RE transport as an advection-diffusion process, we show the result of an equivalent ASCOT5 simulation where the same population is traced in the 3D field until the losses saturated. Good agreement is seen between the model and simulation; as expected, scaling the coefficients by 50% (150%) underestimates (overestimates) the transport.

*Runaway electron evolution.*—The 1D radial-transport solver in the RE modeling framework DREAM [35, 36] is used to consistently evolve the electric field and RE generation – including Dreicer, hot-tail, avalanche, tri-

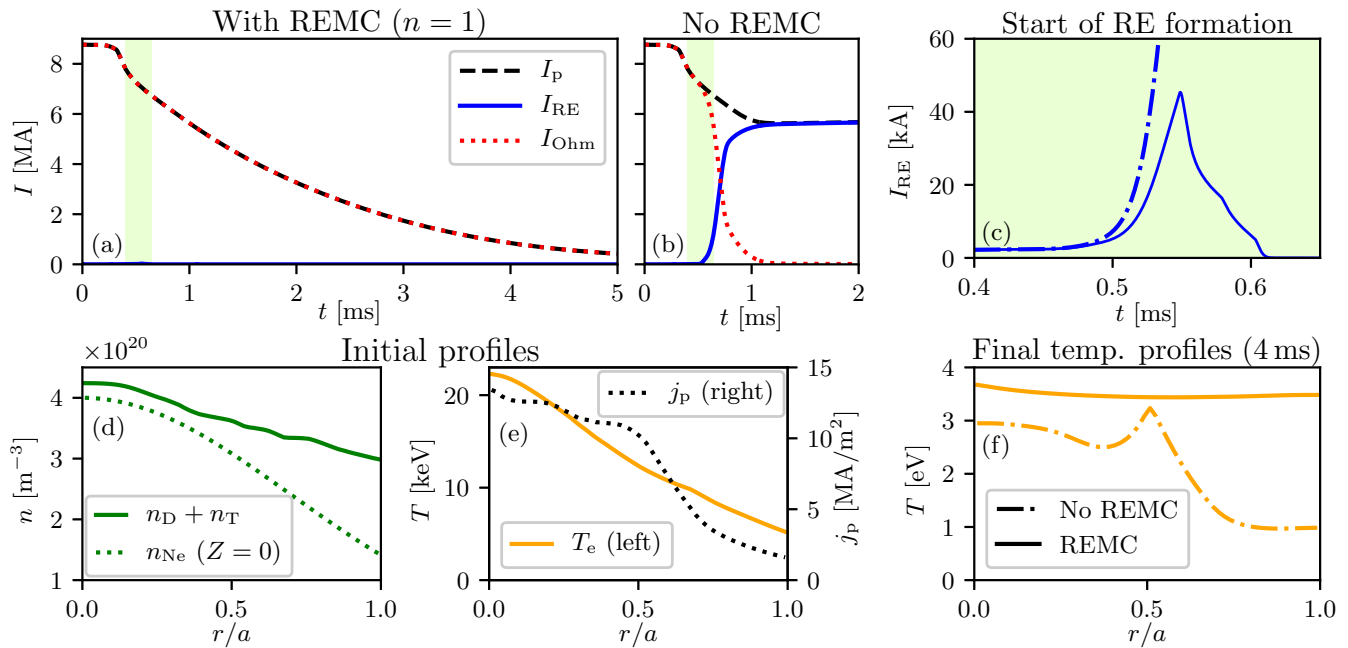


FIG. 4. DREAM simulations of the current evolution with the REMC (a) active and (b) inactive, showing the total plasma current (dashed) with Ohmic (dotted) and RE (solid) components. (c) An expanded view of the RE current in the shaded intervals of (a,b) with the REMC active (solid) and inactive (dot-dashed). Initial profiles of the (d) deuterium + tritium and neutral neon densities and (e) electron temperature and total current density. (f) Final temperature profiles at  $t = 4$  ms.

tium beta decay, and inverse Compton scattering source terms – throughout the disruption. DREAM’s fluid RE transport model, based on [37], simulates the effects of the REMC: time-dependent transport coefficients from ASCOT5 are mapped to  $I_p(t)$  – as in NIMROD (Fig. 2(a)) – and interpolated in the DREAM simulation based on the instantaneous value. A comparison of the total RE currents in Fig. 4(a) and (b), with and without the REMC, shows that the REMC effectively inhibits RE formation. As the CQ begins at  $t \approx 0.5$  ms, a  $\sim 2$  kA hot-tail seed rapidly grows (Fig. 4(c)). With the REMC *inactive*, over 60% ohmic-to-RE current conversion is observed, similar to that seen in previous simulations [2]; average/maximum RE energies attained are  $\sim 8$  MeV/69 MeV, with 90% of REs having energies  $< 17$  MeV.<sup>3</sup> However, with the REMC *active*, the RE dissipation rate due to transport surpasses the growth rate at  $t \approx 0.55$  ms, and the RE current rapidly diminishes after a short transient  $I_{RE} \sim 50$  kA.

These DREAM simulations, performed in the fully fluid mode, are initiated with the plasma profiles shown in Fig. 4(d) and (e). In the first  $t_{TQ} = 0.27$  ms of the simulation, an exponential temperature decrease is prescribed for the TQ, corresponding to an initial drop in the

central temperature from  $\sim 20$  keV to 100 eV. Afterward, the temperature evolution is calculated from power balance, including Ohmic heating, radiation losses, and heat diffusion due to magnetic field perturbations, assuming  $|\delta B/B| = 3 \times 10^{-3}$  (Fig. 2(b)). The effect of the REMC on the final temperature profile is shown in Fig. 4(f); these agree with NIMROD results within a factor of two.

The maximum RE current is highly sensitive to the magnetic energy available for dissipation, determined by the conducting geometry around the plasma. The magnetic boundary surface in DREAM is placed at  $r/a = 1.19$ , enclosing a poloidal magnetic energy of 52.8 MJ, slightly larger than the 52.3 MJ calculated in COMSOL. Note that small changes in this energy can lead to significant changes in the peak current, e.g.  $\Delta r/a \approx +1\% \rightarrow \Delta I_{RE} \approx +50\%$ . The DREAM simulations also use a finite resistive-wall time of 50 ms, consistent with SPARC’s double-walled VV, allowing additional magnetic energy to diffuse into the domain.

In SPARC, the TQ duration is estimated to vary between  $t_{TQ} = 0.1$ – $1$  ms [2, 38], with hot-tail generation increasing with decreasing  $t_{TQ}$ . For  $t_{TQ} = 0.1$  ms, a hot-tail RE current forms, reaching  $\sim 1.2$  MA at  $t \approx 0.5$  ms, but then dissipates quickly by  $t \approx 0.55$  ms. In this simulation, RE transport during the TQ is estimated using a (conservative) RE diffusivity  $(c/v_{te})a^2/t_{TQ} \approx 9000$  m<sup>2</sup>/s, with  $v_{te}$  the electron thermal speed at 20 keV.

The robustness of the result is further tested by artificially reducing transport coefficients in our baseline case by 90%, yielding a RE current spike of only 150 kA

<sup>3</sup> Synchrotron and bremsstrahlung power loss mechanisms are included in DREAM. Drift orbit losses are not included in DREAM explicitly, but rather implicitly through the transport coefficients calculated with ASCOT5.

which dissipates within 0.1 ms of the peak. In another series of NIMROD + ASCOT5 + DREAM simulations, the induced REMC current is halved, yielding a transient  $I_{\text{RE}} \approx 2 \text{ MA}$  at  $t = 0.75 \text{ ms}$ , but the RE beam is dissipated completely by  $t = 0.87 \text{ ms}$ . The striking difference between the maximum  $I_{\text{RE}}$  in the two cases – i.e.  $(A, D) \times 10\%$  vs  $I_{\text{coil}} \times 50\%$  – is due to a delayed onset and shallower penetration of magnetic perturbations in the latter.

Lastly, we address the potential effect of a core magnetic island (Fig. 2(e–g)), where REs could be confined. Simulations with  $A = 0$  and  $D = 0$  inside  $r \leq 4 \text{ cm}$  yields  $I_{\text{RE}} \approx 2 \text{ MA}$  within that region. However, removing all RE transport is excessively conservative; not only would drifts due to the induced electric field [39] cause some REs to escape the island, but the high current density – corresponding to safety factors  $q \ll 1$  and  $\ell_i \gg 1.5$  – will very likely never develop due to the self-regulating kink instability [8, 40]; the self-consistent modeling of which is outside the scope of this study.

*Discussion.*—These promising results have motivated our team to move forward with the engineering design of the  $n = 1$  REMC. Here, we discuss practical requirements of the coil and its impact on tokamak operation.

The REMC will experience various electromechanical stresses and forces. The  $n = 1$  configuration introduces a large sideways force ( $\leq 15 \text{ MN}$ ) due to oppositely directed currents in the two vertical legs. The present plan is to mount the REMC close to the vertical stability coils, and structural analysis is underway. Net-force-free  $n = 1$  alternatives are also under evaluation. Furthermore, full RE suppression might be achieved at a lower maximum REMC current than that specified here; this will be explored both through simulations and as part of the REMC’s experimental program. One option to decrease  $I_{\text{coil}}$  is simply to add an external adjustable resistor to the circuit.

The REMC switch will be located outside the VV for ease of access and radiation protection, but its type has not been decided. The preferred option is a Shockley diode that is passively activated by high voltages unique to the disruption. The absence of any switch (i.e. a continuous coil) or a mechanical switch closed after the  $I_p$  ramp-up has also been considered, but providing protection during ramp-down without inadvertently causing a disruption appears challenging. Preliminary assessments suggest that the resistance required to keep  $I_{\text{coil}}$  at acceptable levels during ramp-down would degrade its performance during disruptions. Furthermore, while the induced voltage from common internal  $m/n = 1/1$  kinks (“sawtooth” crashes) is expected to be negligible, the impact of H-mode’s edge-localized modes on a closed-circuit

coil is unknown and currently under investigation.

The mitigation of REs generated during the low density plasma current ramp-up is a natural extension of the REMC’s function. Unfortunately, the high voltage that would passively activate the REMC during disruptions is not present during a start-up RE event. Powering the REMC using a capacitor bank could be considered if the simpler approach of controlling and ramping-down the RE beam is not possible.

While only the  $n = 1$  REMC configuration is reported in this Letter,  $n = 2$  and 3 designs have also been considered [2]. However, both NIMROD and DREAM simulations indicate reduced and *no* effects of the  $n = 2$  and 3 coils, respectively, on RE formation as the induced transport does not extend far enough into the plasma center (Fig. 3(a,b)), where most REs are generated. Because the engineering requirements of the  $n = 1$  coils are feasible, the  $n = 2$  and 3 designs will not be pursued further. *Summary.*—In this Letter, a non-axisymmetric in-vessel coil, with a toroidal  $n = 1$  geometry, was concluded to be capable of passively preventing post-disruption RE beam formation in the SPARC tokamak. With COMSOL, we modeled the energization of the coil during a realistic CQ. The resulting 3D vacuum magnetic fields were provided as inputs to NIMROD, which simulated the full CQ MHD. Using ASCOT5, we evaluated the transport coefficients of fast electrons in NIMROD’s highly stochastic fields, and the self-consistent evolution of the RE beam, with and without the coil, was simulated with DREAM.

Near-term work will focus on modeling RE impacts on and heating of plasma-facing components. A helical REMC is also under design for installation in the similarly sized DIII-D tokamak [41, 42]. Experimental validation of this Letter’s projected REMC efficiency and exploration of potential (and unknown) side effects will be hugely influential in the decision to close the switch in SPARC.

## ACKNOWLEDGMENTS

The authors thank M Greenwald and P Rodriguez Fernandez for fruitful discussions. This work was supported by Commonwealth Fusion Systems and the Swedish Research Council (Dnr. 2018-03911). We acknowledge the CINECA award, under the ISCRA initiative, for the availability of high performance computing resources and support. This research used resources of the National Energy Research Scientific Computing Center (NERSC), a U.S. Department of Energy Office of Science User Facility operated under Contract No. DE-AC02-05CH11231. Part of the data analysis was performed using the OM-FIT integrated modeling framework [43].

---

[1] T. Hender, J. Wesley, J. Bialek, A. Bondeson, A. Boozer, R. Buttery, A. Garofalo, T. Goodman, R. Granetz,

Y. Gribov, O. Gruber, M. Gryaznevich, G. Giruzzi,

- S. Günter, N. Hayashi, P. Helander, C. Hegna, D. Howell, D. Humphreys, G. Huysmans, A. Hyatt, A. Isayama, S. Jardin, Y. Kawano, A. Kellman, C. Kessel, H. Koslowski, R. L. Haye, E. Lazarro, Y. Liu, V. Lukash, J. Manickam, S. Medvedev, V. Mertens, S. Mirnov, Y. Nakamura, G. Navratil, M. Okabayashi, T. Ozeki, R. Paccagnella, G. Pautasso, F. Porcelli, V. Pustovitov, V. Riccardo, M. Sato, O. Sauter, M. Schaffer, M. Shimada, P. Sonato, E. Strait, M. Sugihara, M. Takechi, A. Turnbull, E. Westerhof, D. Whyte, R. Yoshino, H. Zohm, and the ITPA MHD, Disruption and Magnetic Control Topical Group, *Nuclear Fusion* **47**, S128 (2007).
- [2] R. Sweeney, A. Creely, J. Doody, T. Fülöp, D. Garnier, R. Granetz, M. Greenwald, L. Hesslow, J. Irby, V. Izzo, R. La Haye, N. Logan, K. Montes, C. Paz-Soldan, C. Rea, R. Tinguely, O. Vallhagen, and J. Zhu, *Journal of Plasma Physics* 10.1017/S0022377820001129 (2020).
- [3] A. Gurevich, G. Milikh, and R. Roussel-Dupre, *Physics Letters A* **165**, 463 (1992).
- [4] M. Lehnen, K. Aleynikova, P. Aleynikov, D. Campbell, P. Drewelow, N. Eidietis, Y. Gasparyan, R. Granetz, Y. Gribov, N. Hartmann, E. Hollmann, V. Izzo, S. Jachmich, S.-H. Kim, M. Kočan, H. Koslowski, D. Kovalenko, U. Kruezi, A. Loarte, S. Maruyama, G. Matthews, P. Parks, G. Pautasso, R. Pitts, C. Reux, V. Riccardo, R. Roccella, J. Snipes, A. Thornton, and P. de Vries, *Journal of Nuclear Materials* **463**, 39 (2015).
- [5] G. F. Matthews, B. Bazylev, A. Baron-Wiechec, J. Coenen, K. Heinola, V. Kiptily, H. Maier, C. Reux, V. Riccardo, F. Rimini, G. Sergienko, V. Thompson, and A. Widdowson, *Physica Scripta*, 014070 (2016).
- [6] C. Reux, V. Plyusnin, B. Alper, D. Alves, B. Bazylev, E. Belonohy, A. Boboc, S. Brezinsek, I. Coffey, J. Decker, P. Drewelow, S. Devaux, P. C. De Vries, A. Fil, S. Gerasimov, L. Giacomelli, S. Jachmich, E. M. Khilkevitch, V. Kiptily, R. Koslowski, U. Kruezi, M. Lehnen, I. Lupelli, P. J. Lomas, A. Manzanares, A. Martin De Aguilera, G. F. Matthews, J. Mlynář, E. Nardon, E. Nilsson, C. Perez Von Thun, V. Riccardo, F. Saint-Laurent, A. E. Shevelev, G. Sips, and C. Sozzi, *Nuclear Fusion* **55**, 10.1088/0029-5515/55/9/093013 (2015).
- [7] D. Shiraki, N. Commaux, L. Baylor, C. Cooper, N. Eidietis, E. Hollmann, C. Paz-Soldan, S. Combs, and S. Meitner, *Nuclear Fusion* **58**, 056006 (2018).
- [8] C. Paz-Soldan, N. Eidietis, Y. Liu, D. Shiraki, A. Boozer, E. Hollmann, C. Kim, and A. Lvovskiy, *Plasma Physics and Controlled Fusion* **61**, 054001 (2019).
- [9] C. Reux, C. Paz-Soldan, P. Aleynikov, V. Bandaru, O. Ficker, S. Silburn, M. Hoelzl, S. Jachmich, N. Eidietis, M. Lehnen, S. Sridhar, and JET Contributors, *Phys. Rev. Lett.* **126**, 175001 (2021).
- [10] P. J. Catto, J. R. Myra, P. W. Wang, A. J. Wootton, and R. D. Bengtson, *Physics of Fluids B* **3**, 2038 (1991).
- [11] M. Lehnen, S. A. Bozhnikov, S. S. Abdullaev, and M. W. Jakubowski (TEXTOR Team), *Phys. Rev. Lett.* **100**, 255003 (2008).
- [12] N. Commaux, L. Baylor, S. Combs, N. Eidietis, T. Evans, C. Foust, E. Hollmann, D. Humphreys, V. Izzo, A. James, T. Jernigan, S. Meitner, P. Parks, J. Wesley, and J. Yu, *Nuclear Fusion* **51**, 103001 (2011).
- [13] Z. Chen, D. Huang, Y. Luo, Y. Tang, Y. Dong, L. Zeng, R. Tong, S. Wang, Y. Wei, X. Wang, X. Jian, J. Li, X. Zhang, B. Rao, W. Yan, T. Ma, Q. Hu, Z. Yang, L. Gao, Y. Ding, Z. Wang, M. Zhang, G. Zhuang, Y. Pan, and Z. J. and, *Nuclear Fusion* **56**, 112013 (2016).
- [14] M. Gobbin, O. Ficker, L. Li, Y. Liu, E. Macusova, T. Markovic, M. Nocente, G. Papp, A. Casolari, N. Lamas, *et al.*, in *APS Division of Plasma Physics Meeting Abstracts*, Vol. 2018 (2018) pp. CP11–094.
- [15] Z. Chen, D. Huang, Y. Luo, al, V. Izzo, Z. Y. Chen, W. C. Kim, and Y. W. Yu, *Nuclear Fusion* **58**, 10.1088/1741-4326/aab2fc (2018).
- [16] Z. F. Lin, Z. Y. Chen, D. W. Huang, J. Huang, R. Tong, Y. N. Wei, W. Yan, D. Li, Q. M. Hu, Y. Huang, H. Y. Yang, Y. Li, X. Q. Zhang, B. Rao, Z. J. Yang, L. Gao, Y. H. Ding, Z. J. Wang, M. Zhang, Y. Liang, Y. Pan, and Z. H. J. and, *Plasma Physics and Controlled Fusion* **61**, 024005 (2019).
- [17] S. Munaretto, B. E. Chapman, B. S. Cornille, A. M. Dubois, K. J. McCollam, C. R. Sovinec, A. F. Almagri, and J. A. Goetz, *Nuclear Fusion* **60**, 046024 (2020).
- [18] R. Yoshino and S. Tokuda, *Nuclear Fusion* **40**, 1293 (2000).
- [19] H. M. Smith, A. H. Boozer, and P. Helander, *Physics of Plasmas* **20**, 10.1063/1.4813255 (2013).
- [20] A. J. Creely, M. J. Greenwald, S. B. Ballinger, D. Brunner, J. Canik, J. Doody, T. Fülöp, D. T. Garnier, R. Granetz, T. K. Gray, C. Holland, N. T. Howard, J. W. Hughes, J. H. Irby, V. A. Izzo, G. J. Kramer, A. Q. Kuang, B. LaBombard, Y. Lin, B. Lipschultz, N. C. Logan, J. D. Lore, E. S. Marmor, K. Montes, R. T. Mumgaard, C. Paz-Soldan, C. Rea, M. L. Reinke, P. Rodriguez-Fernandez, K. Särkimäki, F. Sciortino, S. D. Scott, A. Snicker, P. B. Snyder, B. N. Sorbom, R. Sweeney, R. A. Tinguely, E. A. Tolman, M. Umansky, O. Vallhagen, J. Varje, D. G. Whyte, J. C. Wright, S. J. Wukitch, and J. Zhu, *Journal of Plasma Physics* **86**, 865860502 (2020).
- [21] A. H. Boozer, *Plasma Phys. Control. Fusion* **53**, 84002 (2011).
- [22] COMSOL Inc., COMSOL (2020), <http://www.comsol.com/products/multiphysics/>.
- [23] M. Sugihara, V. Lukash, Y. Kawano, R. Khayrutdinov, N. Miki, A. Mineev, J. Ohmori, H. Ohwaki, D. Humphreys, A. Hyatt, V. Riccardo, D. Whyte, V. Zhogolev, P. Barabaschi, K. Ioki, and M. Shimada, in *Proc. 20th Int. Conf. on Fusion Energy 2004* (Vilamoura, Portugal, 2004) pp. 1–8.
- [24] C. Paz-Soldan, M. J. Lanctot, N. C. Logan, D. Shiraki, R. J. Buttery, J. M. Hanson, R. J. La Haye, J.-K. Park, W. M. Solomon, and E. J. Strait, *Physics of Plasmas* **21**, 072503 (2014), <https://doi.org/10.1063/1.4886795>.
- [25] C. R. Sovinec, A. H. Glasser, T. A. Gianakon, D. C. Barnes, R. A. Nebel, S. E. Kruger, S. J. Plimpton, A. Tarditi, M. S. Chu, and the NIMROD Team, *J. Comput. Phys.* **195**, 355 (2004).
- [26] V. Izzo and I. Joseph, *Nuclear Fusion* **48**, 10.1088/0029-5515/48/11/115004 (2008).
- [27] P. Rodriguez-Fernandez, N. T. Howard, M. J. Greenwald, A. J. Creely, J. W. Hughes, J. C. Wright, C. Holland, Y. Lin, and F. Sciortino, *Journal of Plasma Physics* **86**, 865860503 (2020).
- [28] E. Hirvijoki, O. Asunta, T. Koskela, T. Kurki-Suonio, J. Miettunen, S. Sipilä, A. Snicker, and S. Äkäslompolo, *Computer Physics Communications* **185**, 1310 (2014).
- [29] A. B. Rechester and M. N. Rosenbluth, *Phys. Rev. Lett.*

- 40, 38 (1978).
- [30] G. Papp, M. Drevlak, G. I. Pokol, and T. Fülöp, *Journal of Plasma Physics* **81**, 475810503 (2015).
- [31] K. Särkimäki, E. Hirvijoki, J. Decker, J. Varje, and T. Kurki-Suonio, *Plasma Physics and Controlled Fusion* **58**, 125017 (2016).
- [32] T. Hauff and F. Jenko, *Phys. Plasmas* **16**, 102308 (2009), doi: 10.1063/1.3243494.
- [33] J. R. Myra and P. J. Catto, *Phys. Fluids B: Plasma Phys.* **4**, 176 (1992), doi: 10.1063/1.860431.
- [34] A. H. Boozer and G. Kuo-Petravic, *The Physics of Fluids* **24**, 851 (1981).
- [35] M. Hoppe, O. Embreus, and T. Fülöp, *Computer Physics Communications* **268**, 108098 (2021).
- [36] I. Svenningsson, O. Embreus, M. Hoppe, S. L. Newton, and T. Fülöp, *Physical Review Letters* (2021).
- [37] P. Svensson, O. Embreus, S. L. Newton, K. Särkimäki, O. Vallhagen, and T. Fülöp, *Journal of Plasma Physics* **87**, 10.1017/S0022377820001592 (2021).
- [38] ITER Physics Expert Group on Disruptions, Plasma Control, and MHD, and ITER Physics Basis Editors, *Nuclear Fusion* **39**, 2251 (1999).
- [39] X. Guan, H. Qin, and N. J. Fisch, *Physics of Plasmas* **17**, 092502 (2010), <https://doi.org/10.1063/1.3476268>.
- [40] H. Cai and G. Fu, *Nuclear Fusion* **55**, 022001 (2015).
- [41] C. Dunn and D. Weisberg, *Bulletin of the American Physical Society* (2020), JP13.00033.
- [42] D. Weisberg, C. Paz-Soldan, Y. Liu, A. Welander, and C. Dunn, *Nuclear Fusion* **61**, 106033 (2021).
- [43] O. Meneghini, S. Smith, L. Lao, O. Izacard, Q. Ren, J. Park, J. Candy, Z. Wang, C. Luna, V. Izzo, B. Grierson, P. Snyder, C. Holland, J. Penna, G. Lu, P. Raum, A. McCubbin, D. Orlov, E. Belli, N. Ferraro, R. Prater, T. Osborne, A. Turnbull, and G. Staebler, *Nuclear Fusion* **55**, 083008 (2015).